Materials Chemistry

Cite this: *J. Mater. Chem.*, 2012, **22**, 24386

www.rsc.org/materials

PAPER

Semiconductor amphiphilic block copolymers for hybrid donor–acceptor nanocomposites†

Johannes C. Brendel, Hubertus Burchardt and Mukundan Thelakkat*

Received 21st June 2012, Accepted 31st July 2012
DOI: 10.1039/c2jm34033j

Block copolymers feature unique properties for organizing in a well-defined pattern on length scales of several tenths of nanometers. This special attribute enables the formation of ideal donor and acceptor domains for photovoltaic devices in the size of the exciton diffusion length. Thus we designed an amphiphilic block copolymer, able to act as a hole conductor and to coordinate inorganic semiconductor nanoparticles as electron acceptors. Utilizing controlled radical polymerization techniques, defined polymers were synthesized consisting of triphenylamine pendant groups in the hole conductor block and a hydrophilic polystyrene sulfonate block. This particular combination creates narrowly distributed micelles in aqueous solution exhibiting domain sizes suitable for photovoltaic applications. The strong anionic sulfonate groups offer high loading capacities for modified cationic nanoparticles. To guarantee a broad absorption and good conductivity, we synthesized cationic CdSe nanorods and combined them with our hole conductor micelles. The advantage of high loading combined with the processability from aqueous dispersions promises a novel "green" alternative for preparation of hybrid solar cells with controlled domain sizes in the desired length scale.

Introduction

Considering the last few decades of research a countless number of publications were presented on block copolymers (BCP), due to their unique morphologies with nanoscale domain sizes and highly ordered structures in bulk and solution.[1,2] The self-assembly process of these materials is considered to be ideal for "Bottom-up" approaches towards patterned functional thin films.[3,4]

Referring to photovoltaic devices these unique properties perfectly match the desired interface distance in the range of the exciton diffusion length.[5,6] However, the synthesis of functional BCPs for highly efficient solar cells remains challenging. So far only a few reports could prove the advantages of BCPs on solar cells, including the stability of the equilibrated morphology and improved device efficiency. Hashimoto and co-workers synthesized stiff conjugated block copolymers of poly(3-hexylthiophene) (P3HT) and fullerenes attached to the side chains of a second polythiophene block.[7] As a result the stability of the devices was preserved under long term annealing tests due to the equilibrated morphology. In contrast blends of materials are trapped in a non-equilibrium state and on a long time-scale the morphology reaches an undesirable macrophase separated equilibrium state. We and others have earlier shown the advantages of donor–acceptor BCPs, using perylene as an electron acceptor.[8,9] Here, the copolymer exhibited superior device efficiencies compared to the corresponding blend.[8,10] However, the number of soluble, stable and efficient organic electron acceptors is limited. Promising alternatives are n-type inorganic semiconductor nanoparticles, due to their high stability and electron transport mobilities.[11] Combinations of inorganic semiconductors in various shapes and forms are well studied in blend devices with donor polymers.[12] However due to the strong tendency to aggregate high contents of nanoparticles are necessary to guarantee good charge percolation pathways.[13] While blend devices of homopolymers and nanoparticles suffer from the lack of control of morphology and interface, BCPs featuring coordinative groups are able to organize the particles in microphase domains.[14] Here the amount of particles required can be much less than in usual blends due to advantages of confinement.[15] This is the attractiveness of self-assembled systems compared to usual blends. Despite the various detailed studies on self-assembled hybrid materials,[16–21] to our knowledge only a few reports combine functional hole conductor BCPs with inorganic semiconductors suitable for solar cell applications. Lechman *et al.* prepared hybrid devices utilizing the amphiphilic polymer poly(ethylene oxide)-*b*-polytriphenylamine (PEO-*b*-PTPA), whereat titanium dioxide was hydrolyzed in the PEO-block using sol–gel chemistry precursors.[22] Secondly, hybrid structures could be generated with poly(vinyl-*N*,*N*′-bis(4-methoxyphenyl)-*N*,*N*′-diphenyl-(1,1′-biphenyl)-4,4′-diamine)-*block*-poly(4-vinylpyridine) (PDMTPD-*block*-P4VP). CdSe nanoparticles could be

Applied Functional Polymers, Macromolecular Chemistry I, University of Bayreuth, 95440 Bayreuth, Germany. E-mail: mukundan.thelakkat@uni-bayreuth.de; Fax: +49 921 553109; Tel: +49 921 553108

† Electronic supplementary information (ESI) available. See DOI: 10.1039/c2jm34033j

selectively incorporated into the P4VP phase of the lamellar morphology.[23]

Motivated by the requirement of novel materials for this promising field, we synthesized the new amphiphilic BCP poly-(bis(4-methoxyphenyl)-4′-vinylphenylamine)-*block*-poly(tetrabutylammonium styrene sulfonate) (PDMTPA-*b*-PBu_4N^+SS) (Scheme 1).

PDMTPA is an amorphous hole conductor polymer that has been well-studied by our group before.[24] Hole mobilities up to 5×10^{-5} cm^2 V^{-1} s^{-1} were found.[25] As hydrophilic block we chose PBu_4N^+SS, due to its sufficient solubility and the high charge density even at low pH. As previously reported, the sulfonate groups feature the catalytic crystallization of TiO_2 at room temperature.[26,27] Furthermore, the strong coulomb interactions of the polyelectrolyte enable high loading capacities with oppositely charged nanoparticles, while maintaining a high solubility.[28] The close arrangement of the nanoparticles is crucial for the percolation of charges and conductivity. The desired block copolymer was synthesized by reversible addition fragmentation chain transfer polymerization (RAFT). Therefore, we first needed to optimize the polymerization conditions in order to get well-defined molecular weights and low polydispersities.[23] The sulfonated block was prepared *via* polymerization of the protected monomer, neopentyl styrene sulfonate (NeoSS). This allows the use of common high boiling solvents such as anisole or toluene and the neopentyl group can be easily removed afterwards.[29,30] The resulting amphiphilic polymer was studied for its morphology in aqueous solution by dynamic light scattering (DLS) and transmission electron microscopy (TEM). We combined these micelles with highly crystalline CdSe nanorods to ensure the absorption of visible light and good electron transport. The particles can be modified with aminoethanethiol hydrochloride to get a high positive surface charge gaining solubility in water.[31] Due to the strong attraction to the negatively charged PBu_4N^+SS-block, mixing of both components results in a stable colloidal solution of donor and acceptor materials in water.

Results and discussion

During the last decade RAFT polymerization has become an important technique among the controlled radical polymerizations for macromolecule design.[32–34] But actually there are only a few reports on the polymerization of functional semiconductor monomers.[35] Due to the larger size of these monomers compared to simple styrene or acrylate monomers and the sensitivity against radical oxidation, particular attention has to be paid to the polymerization conditions.

The order of monomer addition is crucial for well-defined block copolymers by RAFT.[36] Especially triphenylamine monomers (TPA) are able to stabilize the propagating radical altering the reactivity of the active chain end. In consequence we first prepared the individual homopolymers PDMTPA and poly(neopentyl styrene sulfonate) (PNeoPSS) and verified their ability to initiate the respective counterpart. Both polymerizations were carried out using 2-cyano-2-propylbenzodithioate as chain transfer agent (CTA) and at 80 °C in anisole, which is a suitable high boiling solvent for both monomers.

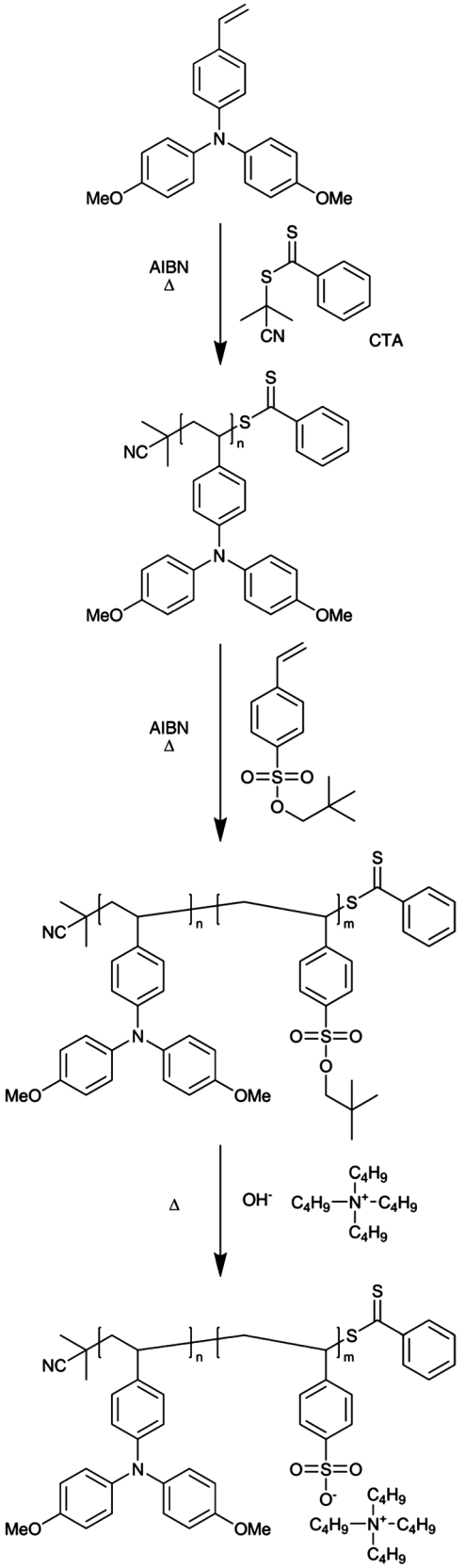

Scheme 1 Synthesis of poly(4,4′-dimethoxytriphenylamine)-*block*-poly(tetrabutylammonium styrene sulfonate) (PDMTPA-*b*-PBu_4N^+SS) using 2-cyano-2-propylbenzodithioate as chain transfer agent (CTA).

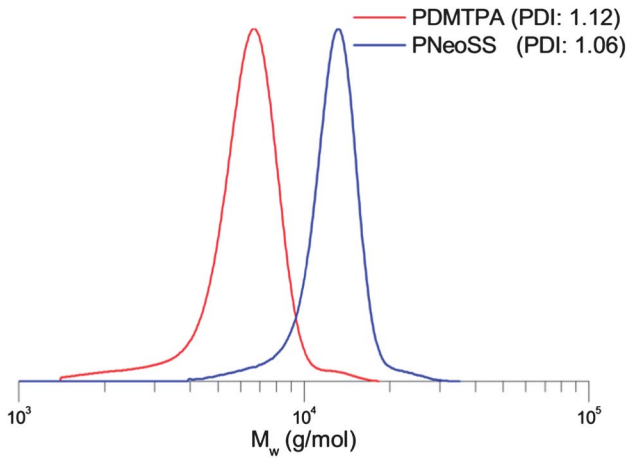

Fig. 1 GPC-plots of the homopolymers poly(bis(4-methoxyphenyl)-4′-vinylphenylamine) (PDMTPA, red) and poly(neopentyl styrene sulfonate) (PNeoSS, blue), eluent: THF, calibration with polystyrene.

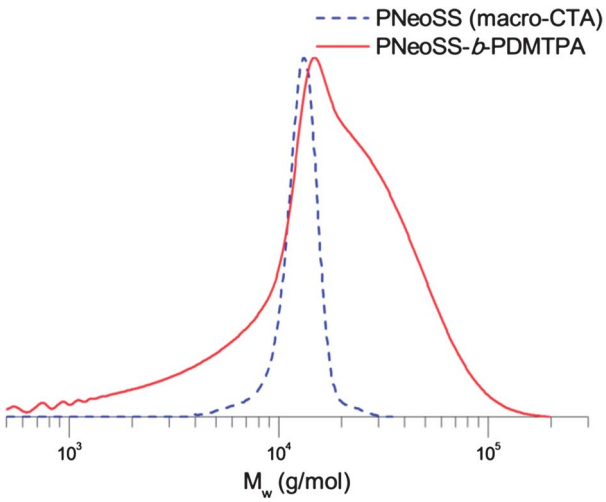

Fig. 2 Comparison of GPC plots of the initiating macro-CTA PNeoSS (dashed line) and the resulting block copolymer PNeoSS-*b*-PDMTPA (continuous line).

Both the resulting homopolymers showed narrow molecular weight distributions (Fig. 1), which implies good control of the RAFT polymerization of the monomers.

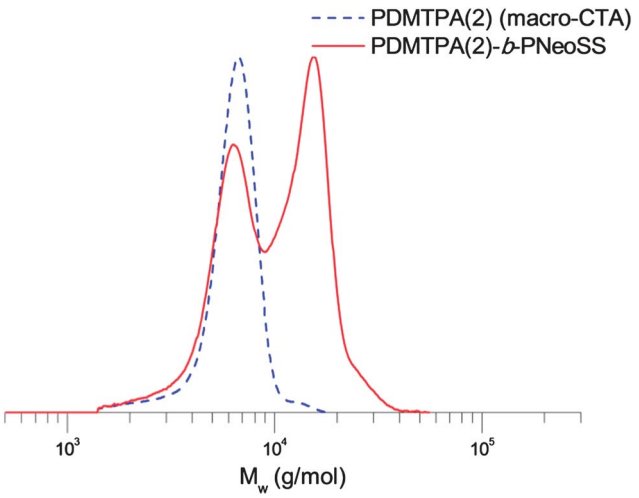

Fig. 3 Comparison of GPC plots of the initiating macro-CTA PDMTPA (dashed line) and the resulting block copolymer PDMTPA-*b*-PNeoSS (continuous line).

Then, we studied the sequential polymerization of DMTPA using the macro-CTA PNeoSS under similar conditions. The GPC trace of sample PNeoSS-*b*-PDMTPA displays no significant shift of the main peak in comparison to the macro-CTA (Fig. 2). Furthermore a broad underlying peak was formed characteristic for a free radical polymerization. This indicates that PNeoSS was not able to initiate the polymerization of DMTPA and a broadly distributed homopolymer was formed in addition to the macro-CTA. Changing the synthesis conditions such as variation of temperature and concentration unfortunately had no influence on this process (Fig. S1 in the ESI†).

Alternatively we started the polymerization of NeoSS as second monomer from PDMTPA as macro-CTA. Here the GPC traces clearly indicated the formation of a block copolymer. However, a second peak was observed at the original elution volume of PDMTPA (Fig. 3). This suggests that a considerable part of the macro-CTA remained unreactive. Keeping a retarded initiation in mind, one could expect a statistical distribution covering the macro-CTA and the associated BCPs, resulting in one broad peak. But a bimodal distribution indicates that the main part of the PDMTPA homopolymer was able to initiate the controlled polymerization of NeoSS, while a second part remained without addition of further monomer units. In

Table 1 Synthesis conditions and characterization for the macro-CTAs and the respective block copolymers

	Monomer/CTA/AIBN ratio	*T*	Solvent	M_n (kg mol^{-1})[a]	M_{p1} (kg mol^{-1})[a,b]	M_{p2} (kg mol^{-1})[a,b]	PDI
Macro-CTA							
PDMTPA(1)	50/1/0.2	60 °C	Anisole	3.21	3.66	—	1.09
PDMTPA(2)	50/1/0.2	80 °C	Anisole	5.80	6.64	—	1.12
PDMTPA(3)	50/1/0.2	100 °C	Anisole	4.97	5.73	—	1.11
PDMTPA(4)	50/1/0.2	60 °C	Benzene	4.52	4.94	—	1.07
BCP							
PDMTPA(1)-*b*-PNeoSS	100/1/0.4	80 °C	Anisole	4.78	4.06	8.55	1.30
PDMTPA(2)-*b*-PNeoSS	100/1/0.4	80 °C	Anisole	8.67	6.31	15.23	1.28
PDMTPA(3)-*b*-PNeoSS	100/1/0.4	80 °C	Anisole	8.77	5.73	15.47	1.34
PDMTPA(4)-*b*-PNeoSS	100/1/0.4	80 °C	Anisole	11.55	5.00	18.95	1.37

[a] GPC was calibrated with polystyrene as standard. [b] M_p was defined as the molecular weight of single peaks.

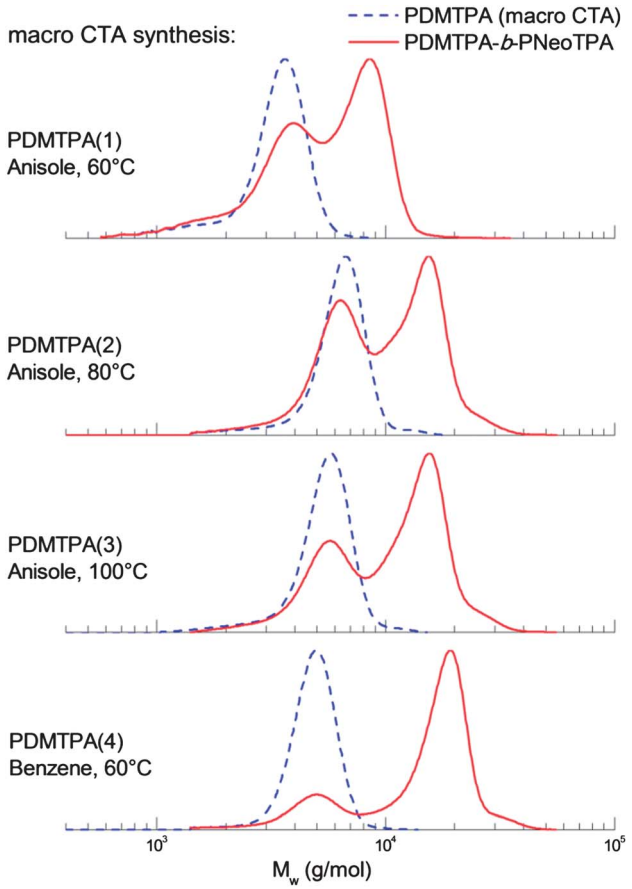

Fig. 4 GPC-traces of the samples PDMTPA(1)-*b*-PNeoSS, PDMTPA(2)-*b*-PNeoSS, PDMTPA(3)-*b*-PNeoSS and PDMTPA(4)-*b*-PNeoSS (solid lines) and the respective macro-CTAs (dashed lines). The variations in synthesis of the macro-CTA are shown on the left, while the BCP was formed under similar conditions (Experimental section).

consequence, the functional chain transfer end group of the PDMTPA must be partially disabled or lost. As no intermediate steps of purification are involved in the macro-CTA synthesis, this process must already occur during the polymerization of DMTPA. For verification we altered the conditions of the macro-CTA synthesis and consequently tested the macro-initiator efficiency of the macro-CTAs prepared in different solvents and at different temperatures keeping the concentration and ratio of components the same. Thus, the temperature was varied from 60 to 100 °C and secondly the polarity of the medium was changed. A summary of these reactions and the corresponding polymer characteristics are given in Table 1.

The reduced reaction temperature (60 °C) in anisole of the macro-CTA PDMTPA(1) reduced the polymerization rate, so that only a conversion of 44% was reached after 22 h. All other samples were stopped at higher conversions of 55–60%, yielding similar molecular weights and narrow distributions. Those macro-CTAs were then employed in the polymerization of NeoSS under conditions summarized in Table 1. The GPC plots of the resulting BCPs and the respective macro-CTAs are shown in Fig. 4.

By raising the temperature for the macro-CTA synthesis from 60 °C to 80 °C the amount of unreactive PDMTPA increased slightly. Considerable improvements were observed at a high temperature of 100 °C, but still a substantial part of the macro-CTA remained unreactive in polymerization using macro-CTA PDMTPA(3). The best result was obtained with macro-CTA PDMTPA(4) by changing the solvent from anisole to benzene and thus reducing the polarity of the surrounding medium. Despite a small part of unreacted homopolymer was still visible, a low polydispersity index (PDI) of 1.37 was reached for the as-synthesized BCP. The final polymer PDMTPA(4)-*b*-PNeoSS was purified by preparative GPC to remove the last traces of the homopolymer. The GPC trace of the final polymer is shown in Fig. 5. These results obviously prove the influence of the initial macro-CTA synthesis on the final initiator efficiency.

Further evidence of a loss of the chain transfer agent was attained by matrix-assisted laser desorption/ionization time-of-flight (MALDI-TOF) measurements, which provides detailed

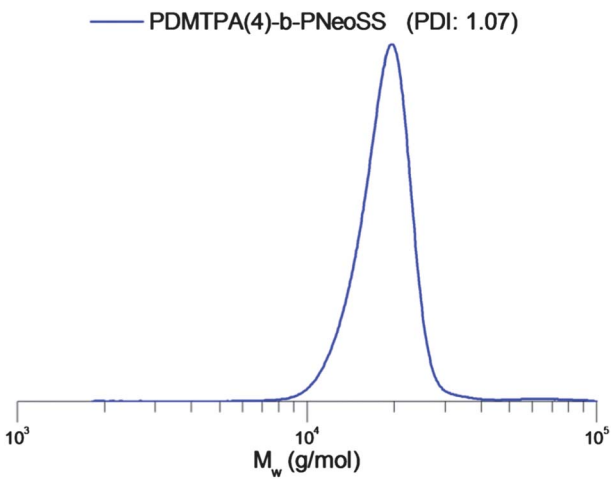

Fig. 5 GPC-trace of the purified sample PDMTPA(4)-*b*-PNeoSS.

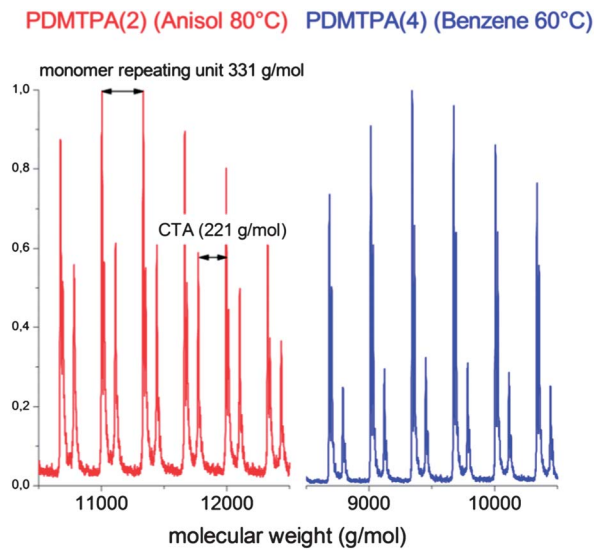

Fig. 6 Matrix-assisted laser desorption/ionization time-of-flight measurements of macro-CTA PDMTPA(2) and PDMTPA(4). The major peak series corresponds to the macro-CTA and the minor one to the homopolymer with dead chain ends.

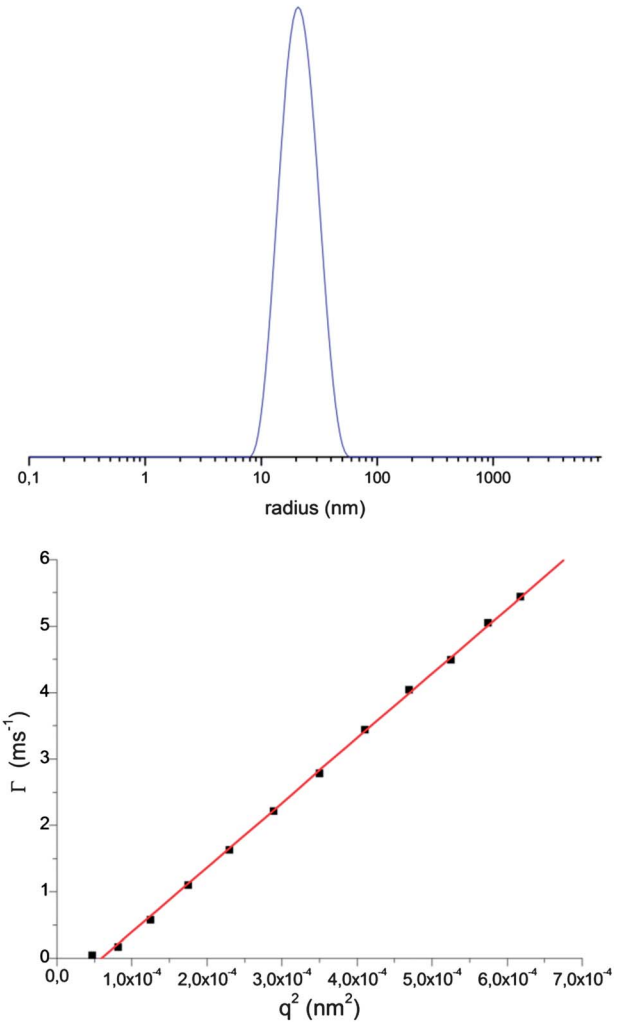

Fig. 7 A representative distribution of micelles for an angle of 120° (top) and the plot of Plot of Γ against q^2 for various measured angles (bottom).

information on the end-group distribution. For comparison the measurements of macro-CTAs PDMTPA(2) and PDMTPA(4) are plotted in Fig. 6. The full MALDI spectra of all samples are given in the ESI (Fig. S2–S5†). The second peak series clearly indicate a change in the polymer end groups. The difference of 221 g mol^{-1} correlates well with the loss of the chain transfer agent 2-cyano-2-propylbenzodithioate. Furthermore comparing the intensities of the second peak the ratio of active species to dead chain end moieties decreases from macro-CTA PDMTPA(2) to PDMTPA(4). This is in good agreement with the GPC traces of the block copolymers, where the part of unreactive homopolymer decreases, too.

The lost CTA is possibly caused by the formation of additional free radicals, which terminate the active polymer. As the polymer distribution remains narrow, this process seems to be suppressed at the beginning of the polymerization, but increases drastically with higher conversion. For styrene monomers self-initiation and radical formation is already well studied and we assumed a similar process for this system.[2,37] Therefore the polymerization was examined under similar conditions, without using any AIBN initiator. GPC traces at different reaction times evidently present the formation of oligomers first and higher molecular weight polymers after 23 h (Fig. S6 in the ESI†). In comparison to the self-initiation radical polymerization of styrene, here first a cycloaddition step is involved.[37] The electron donating effect of the nitrogen in the triphenylamine monomer and the increased number of active phenyl rings enhance this effect. Free hydrogen radicals are created in this reaction to retain the aromaticity in the resulting molecule after the cycloaddition, which may start or quench a radical polymerization. However, for a detailed mechanism further studies have to be performed to get insight into this phenomenon, which are not part of this research. But the presented results certainly depict the importance of detailed kinetic studies in optimization of synthesis of functional block copolymers.

With a well-defined polymer in hand, we consequently studied the assembly and coordination properties of PDMTPA-*b*-PSS. After deprotection of the sulfonate groups, the BCP showed a distinct amphiphilic character. The complete deprotection was confirmed by NMR analysis (Fig. S7 in the ESI†). Thus the polymer showed micelle formation in aqueous solutions. These assembly structures were characterized by dynamic light scattering (DLS) to obtain the hydrodynamic radius R_h. For consistent values we measured the decay rate Γ, calculated from the autocorrelation function (1. order of cumulant fit), for multiple angles θ and plotted it against q^2 with $q = 4\pi n/\lambda \times \sin(\theta/2)$ (n: refractive index; λ: wavelength of the laser). The respective linear slope of the plot is correlated to the diffusion coefficient D by $\Gamma = Dq^2$. With D the hydrodynamic radius R_h can be calculated as $R_h = (k_B T)/(6\pi\eta D)$ (k_B: Boltzmann constant; T: temperature; η: viscosity of the medium).

The plot in Fig. 7 clearly displays a linear relation between Γ and q^2. From the slope a hydrodynamic radius R_h of 22 nm ± 0.23 nm was determined. While this value reflects the size of the micelles in solution, including the hydrated polyelectrolyte shell,

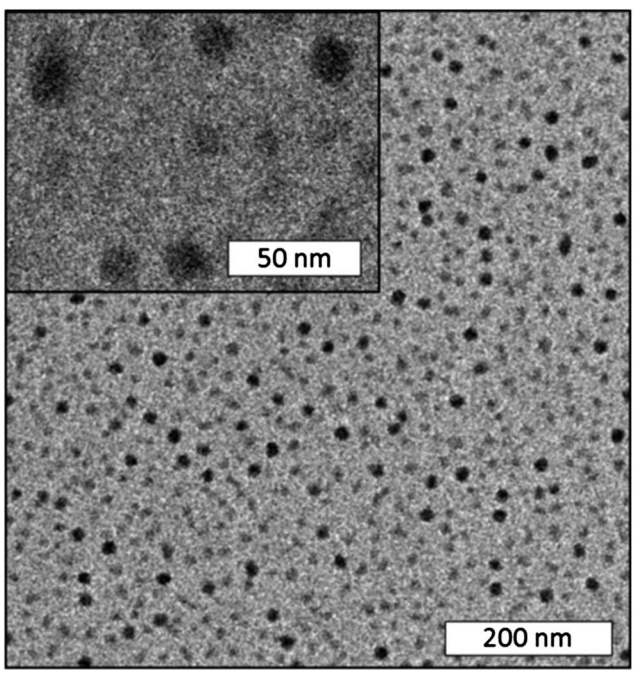

Fig. 8 Transmission electron micrographs of the dried micelles stained with ruthenium tetroxide.

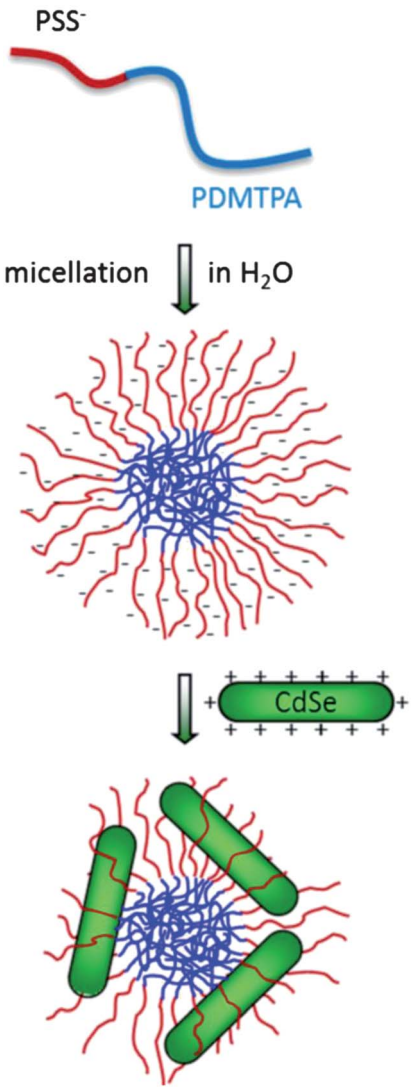

Fig. 9 General preparation scheme of hybrid colloidal composites.

adjacent transmission electron micrographs (TEM) of the dried micelles stained with ruthenium tetroxide reveal a core diameter of approximately 16 nm (Fig. 8).

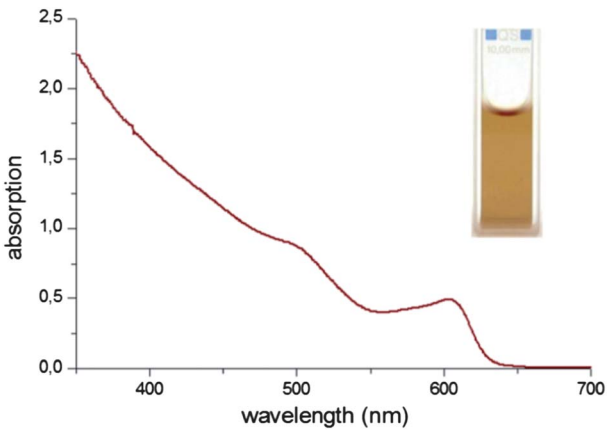

Fig. 10 Absorption of the prepared CdSe nanoparticles with 2-aminoethanethiol ligand in water (0.5 mg ml^{-1}).

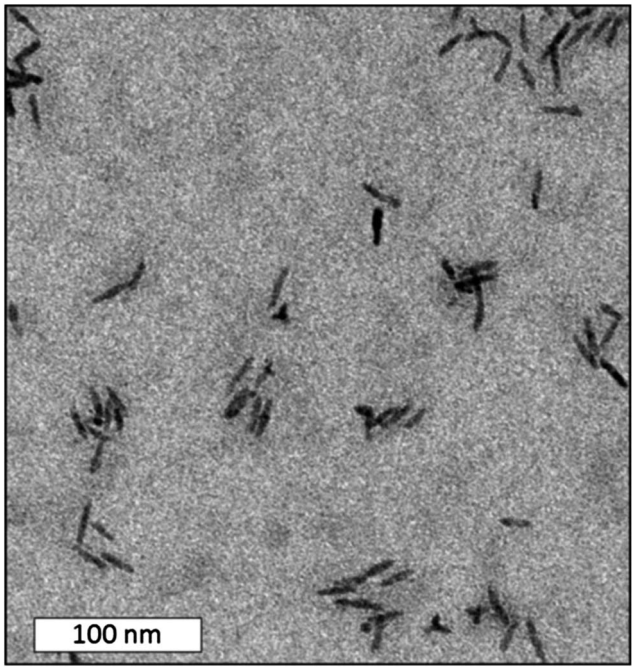

Fig. 11 Transmission electron micrographs of the CdSe nanorods attached to the block copolymer micelles.

The respective individual sizes of the core and the shell (~14 nm) are in good agreement with theoretical values for a coiled solid PDMTPA-block and a highly stretched PBu_4N^+SS-block, which is characteristic for strong polyelectrolytes in deionised water.[38] Aqueous dispersions of those micelles are stable and showed no precipitation, even after storage under ambient conditions for several months.

We have studied earlier the coordination capabilities of PSS containing spherical polyelectrolyte brushes.[26,28] Building upon this experience, we studied the coordination abilities of the PDMTPA-*b*-PBu_4N^+SS micelles. In contrast to the spherical colloidal particles, no time-consuming solvent exchange is necessary, as the micelles can be freeze dried and well dispersed in various suitable polar solvents. Non-toxic solvents such as water or alcohols are highly preferred in technological applications. Therefore, we focused on a system using water soluble semiconductor nanoparticles.[39] Furthermore, to guarantee an efficient absorption of the visible light, the particles need to have good absorption coefficients in this range. CdSe nanoparticles fulfil these requirements and they are well studied in solar cells.[11,12] A general scheme of this colloidal assembly route is shown in Fig. 9.

Recently Zentel *et al.* presented a comparable BCP in combination with CdSe quantum dots for application in light emitting devices.[40] A similar colloidal arrangement was shown by Winnik *et al.* using commercial block copolymers.[41] The synthesis of CdSe nanoparticles with various shapes and high crystallinity is well controlled using various phosphonic acid ligands.[42,43] To enable the solubility in water we exchanged this ligand with the hydrophilic 2-aminoethanethiol (AET) according to Krauss *et al.*[31] The resulting nanoparticles exhibit a good solubility in water and good absorption up to 630 nm (Fig. 10). According to

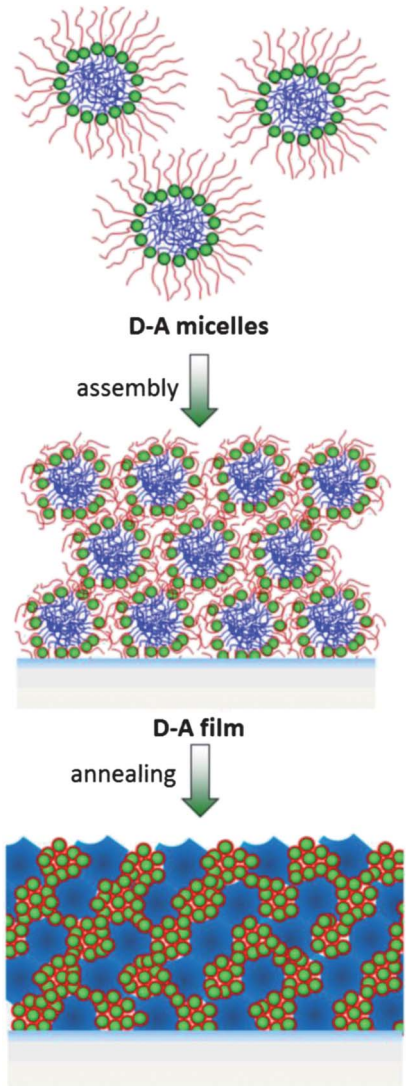

Fig. 12 General scheme for the preparation of a donor–acceptor (D–A) microstructure from hybrid colloidal nanocomposites.

the literature the HOMO and LUMO levels of PDMTPA are at 5.0 eV and 1.8 eV respectively.[6] CdSe nanoparticles of similar shape typically have a conduction band edge at 6.2 eV and a valence band edge at 4.4 eV.[44] Thus this system fulfil the requirements for charge transfer.

Transmission electron micrographs show uniformly distributed CdSe nanoparticles with an average diameter of 5 nm and length of 21 nm (Fig. S8 in the ESI†). The positively charged AET ligands not only convey the water solubility, but also yield a strong coulombic interaction between the nanoparticles and the negatively charged sulfonate groups. By mixing both solutions the nanocrystals immediately attach to the negative charged micelles. The strong driving force is attributed to the enthalpy benefit from the release of multiple counterions by exchanging with a single particle. These strong interactions enable a high loading capacity in comparison to uncharged polymers like polyvinylpyridine, while maintaining the stability of the dispersions.[28] Composites of the CdSe nanoparticles and the PDMTPA-*b*-PBu_4N^+SS micelles are shown in the transmission electron micrographs in Fig. 11. The weight ratio of nanoparticles against polymer was as high as 1 : 1.

Only a few single nanoparticles are obviously seen in the images, which confirm the strong interaction. The high loading facilitates a better packing of the nanoparticles, which is crucial for high charge carrier mobility.[45] A major advantage of this separate synthesis of polymer and inorganic semiconductor is the variability of the nanoparticle synthesis. In literature the preparation of several highly crystalline nanoparticles is well-known and they all can be combined with these micelle structures by electrostatic interaction.[46]

Finally the resulting donor–acceptor (D–A) micelles can be used to prepare devices with microstructures on the length scale of the exciton diffusion length. A general scheme of this concept with spherical nanoparticles is shown in Fig. 12. The nanocomposite micelles can be assembled onto a conducting substrate and dried to get a smooth film, which can be annealed or pressed above T_g to get bicontinuous domains. The amorphous PDMTPA softens and forms a continuous phase. Simultaneously the particles aggregate to create the required percolation once the concentration increases on drying and annealing as shown in Fig. 12. In such a system the charge transfer and transport required for a solar cell are feasible.

Conclusion

The ability of block copolymers to create domains in the nanometer scale reveals them to be ideal for structured organic or hybrid solar cells. Here we developed an innovative colloidal organization of inorganic semiconductors and semiconductor amphiphilic block copolymers. The polymer consists of a well-known hole conductor block and a water soluble styrene sulfonate block, able to coordinate nanoparticles by electrostatic interaction. We optimized the synthesis conditions to accomplish narrow distributions and create well-defined micelle dispersions. Crucial in this context are the order of monomer addition and the reactivity of the triphenylamine monomer. The latter resulted in the loss of the chain transfer agent during the homopolymerization. This caused bimodal distributions during the block copolymer formation. By altering the temperature and solvent polarity the side reaction could be minimized and thus the ratio of unreactive homopolymer reduced. After hydrolysis of the sulfonate protection groups the block copolymer formed uniform and stable micelles in aqueous solutions. The highly charged sulfonate groups are strong coordinating groups especially for electrostatic interaction with charged nanoparticles. Ideal semiconductors for this approach are CdSe nanorods. They combine both good absorption in the visible spectrum of light and high electron mobility. By exchanging the typical phosphine ligands with a positive charged aminoethanethiol the particles can be attached to our hole conductor micelles. In consequence we created semiconductor colloids including both a donor material and an acceptor. The domain sizes are defined by the micelle core and the nanoparticle size, which can be adjusted in individual reactions. As the system is based on an aqueous dispersion no hazardous solvents are necessary for processing enabling large scale industrial fabrication. The strong electrostatic interaction of the sulfonate polymer allows high loading capacities while maintaining the good solubility. In combination

with other polymerization techniques all kind of functional polymers such as polythiophenes or low band-gap polymers can be integrated into this environmentally benign processing of devices from water. Furthermore various inorganic semiconductors such as TiO_2 or $CuInS_2$ are interesting alternatives which can easily be incorporated. In conclusion this approach opens a promising pathway towards defined donor–acceptor hybrid systems using semiconductor amphiphilic block copolymers.

Acknowledgements

Financial support from SFB 840 and Bayerische Eliteförderung is kindly acknowledged. Furthermore we thank Melanie Förtsch and Katharina Neumann for the TEM and MALDI measurements respectively.

References

1 S. Förster and M. Antonietti, *Adv. Mater.*, 1998, **10**, 195.
2 P. J. Flory, *J. Am. Chem. Soc.*, 1937, **59**, 241.
3 J. Weickert, R. B. Dunbar, H. C. Hesse, W. Wiedemann and L. Schmidt-Mende, *Adv. Mater.*, 2011, **23**, 1810.
4 J. Y. Cheng, C. A. Ross, H. I. Smith and E. L. Thomas, *Adv. Mater.*, 2006, **18**, 2505.
5 P. D. Topham, A. J. Parnell and R. C. Hiorns, *J. Polym. Sci., Part B: Polym. Phys.*, 2011, **49**, 1131.
6 M. Sommer, S. Huettner and M. Thelakkat, *J. Mater. Chem.*, 2010, **20**, 10788.
7 S. Miyanishi, Y. Zhang, K. Tajima and K. Hashimoto, *Chem. Commun.*, 2010, **46**, 6723.
8 M. Sommer, A. S. Lang and M. Thelakkat, *Angew. Chem., Int. Ed.*, 2008, **47**, 7901.
9 Q. Zhang, A. Cirpan, T. P. Russell and T. Emrick, *Macromolecules*, 2009, **42**, 1079.
10 M. Sommer, S. M. Lindner and M. Thelakkat, *Adv. Funct. Mater.*, 2007, **17**, 1493.
11 M. Skompska, *Synth. Met.*, 2010, **160**, 1.
12 W. U. Huynh, J. J. Dittmer and A. P. Alivisatos, *Science*, 2002, **295**, 2425.
13 K. F. Jeltsch, M. Schädel, J.-B. Bonekamp, P. Niyamakom, F. Rauscher, H. W. A. Lademann, I. Dumsch, S. Allard, U. Scherf and K. Meerholz, *Adv. Funct. Mater.*, 2012, **22**, 397.
14 Y. Lin, A. Boker, J. He, K. Sill, H. Xiang, C. Abetz, X. Li, J. Wang, T. Emrick, S. Long, Q. Wang, A. Balazs and T. P. Russell, *Nature*, 2005, **434**, 55.
15 C.-P. Li, K.-H. Wei and J. Y. Huang, *Angew. Chem., Int. Ed.*, 2006, **45**, 1449.
16 A. C. Balazs, T. Emrick and T. P. Russell, *Science*, 2006, **314**, 1107.
17 N. Haberkorn, M. C. Lechmann, B. H. Sohn, K. Char, J. S. Gutmann and P. Theato, *Macromol. Rapid Commun.*, 2009, **30**, 1146.
18 S.-W. Yeh, K.-H. Wei, Y.-S. Sun, U.-S. Jeng and K. S. Liang, *Macromolecules*, 2005, **38**, 6559.
19 A. Haryono and W. H. Binder, *Small*, 2006, **2**, 600.
20 Y. Lin, V. K. Daga, E. R. Anderson, S. P. Gido and J. J. Watkins, *J. Am. Chem. Soc.*, 2011, **133**, 6513.
21 Q. Zhang, S. Gupta, T. Emrick and T. P. Russell, *J. Am. Chem. Soc.*, 2006, **128**, 3898.
22 M. C. Lechmann, S. A. L. Weber, J. Geserick, N. Husing, R. Berger and J. S. Gutmann, *J. Mater. Chem.*, 2011, **21**, 7765.
23 S. Maria, A. S. Susha, M. Sommer, D. V. Talapin, A. L. Rogach and M. Thelakkat, *Macromolecules*, 2008, **41**, 6081.
24 S. Hüttner, M. Sommer, U. Steiner and M. Thelakkat, *Appl. Phys. Lett.*, 2010, **96**, 073503.
25 E. M. Barea, G. Garcia-Belmonte, M. Sommer, S. Hüttner, H. J. Bolink and M. Thelakkat, *Thin Solid Films*, 2010, **518**, 3351.
26 J. C. Brendel, Y. Lu and M. Thelakkat, *J. Mater. Chem.*, 2010, **20**, 7255.
27 Y. Lu, M. Hoffmann, R. S. Yelamanchili, A. Terrenoire, M. Schrinner, M. Drechsler, M. W. Möller, J. Breu and M. Ballauff, *Macromol. Chem. Phys.*, 2009, **210**, 377.
28 R. S. Yelamanchili, Y. Lu, T. Lunkenbein, N. Miyajima, L.-T. Yan, M. Ballauff and J. Breu, *Small*, 2009, **5**, 1326.
29 H. Okamura, Y. Takatori, M. Tsunooka and M. Shirai, *Polymer*, 2002, **43**, 3155.
30 S. C. Miller, *J. Org. Chem.*, 2010, **75**, 4632.
31 J. M. Haremza, M. A. Hahn, T. D. Krauss, S. Chen and J. Calcines, *Nano Lett.*, 2002, **2**, 1253.
32 H. Kakwere and S. Perrier, *Polym. Chem.*, 2011, **2**, 270.
33 M. Siauw, B. S. Hawkett and S. Perrier, *J. Polym. Sci., Part A: Polym. Chem.*, 2012, **50**, 187.
34 G. Moad, E. Rizzardo and S. H. Thang, *Polymer*, 2008, **49**, 1079.
35 G. Moad, M. Chen, M. Haussler, A. Postma, E. Rizzardo and S. H. Thang, *Polym. Chem.*, 2011, **2**, 492.
36 Y. K. Chong, J. Krstina, T. P. T. Le, G. Moad, A. Postma, E. Rizzardo and S. H. Thang, *Macromolecules*, 2003, **36**, 2256.
37 F. R. Mayo, *J. Am. Chem. Soc.*, 1968, **90**, 1289.
38 S. Förster, N. Hermsdorf, C. Bottcher and P. Lindner, *Macromolecules*, 2002, **35**, 4096.
39 R. Sondergaard, M. Helgesen, M. Jorgensen and F. C. Krebs, *Adv. Energy Mater.*, 2011, **1**, 68.
40 J. Kwak, W. K. Bae, M. Zorn, H. Woo, H. Yoon, J. Lim, S. W. Kang, S. Weber, H.-J. Butt, R. Zentel, S. Lee, K. Char and C. Lee, *Adv. Mater.*, 2009, **21**, 5022.
41 M. Wang, S. Kumar, A. Lee, N. Felorzabihi, L. Shen, F. Zhao, P. Froimowicz, G. D. Scholes and M. A. Winnik, *J. Am. Chem. Soc.*, 2008, **130**, 9481.
42 W. Wang, S. Banerjee, S. Jia, M. L. Steigerwald and I. P. Herman, *Chem. Mater.*, 2007, **19**, 2573.
43 Z. A. Peng and X. Peng, *J. Am. Chem. Soc.*, 2000, **123**, 183.
44 S. A. McClure, B. J. Worfolk, D. A. Rider, R. T. Tucker, J. A. M. Fordyce, M. D. Fleischauer, K. D. Harris, M. J. Brett and J. M. Buriak, *ACS Appl. Mater. Interfaces*, 2009, **2**, 219.
45 C.-P. Li, K.-H. Wei and J. Y. Huang, *Angew. Chem., Int. Ed.*, 2006, **45**, 1449.
46 M. Kruszynska, H. Borchert, J. Parisi and J. Kolny-Olesiak, *J. Am. Chem. Soc.*, 2010, **132**, 15976.